

S-GAI: Spectral Geometry-Aware Initialization for Sigmoidal MLPs

From Dataset Geometry to Network Weights

Yi-Shan Chu

easonchu@stat.sinica.edu.tw

Institute of Statistical Science, Academia Sinica, Taipei, Taiwan (R.O.C.)

Abstract. Classical universal approximation theorems establish the expressive power of sigmoidal multilayer perceptrons, but they do not prescribe how initial weights should encode the geometry of a data distribution. We propose S-GAI, a spectral geometry-aware initialization framework for one-hidden-layer sigmoidal MLPs. Starting from the constructive idea that sigmoid units can act as smooth half-space gates, we move from hand-specified planar geometry to class-wise spectral geometry estimated from image data. For each class, SVD provides a mean, principal directions, and spectral scales. An energy threshold selects the retained directions, and each retained direction is represented by two sigmoid gates. These class-specific gates form a shared hidden layer initialized directly from the training set. We also formulate a SVD-based subspace classifier as a non-neural geometric reference, which tests whether the estimated spectral class geometry is already discriminative before being embedded into the MLP. Experiments on MNIST, Fashion-MNIST, and a more challenging CIFAR-10 test show that the S-GAI-initialized MLP starts from a substantially more informative hidden state than Xavier initialization and reaches comparable final accuracy under full training. When the hidden layer is frozen, training only the output layer still gives stronger performance than frozen random gates, providing evidence that S-GAI effectively embeds class-wise spectral geometry into the MLP.

Keywords: Geometry-aware initialization · Sigmoidal MLP · SVD · Universal approximation · MNIST · Fashion-MNIST · CIFAR-10 · Image Classification

1 Introduction

The universal approximation theorem (UAT) [3] is often read as an expressive-power statement: with enough hidden units, a sigmoidal MLP can approximate any continuous target on a compact domain. In its classical form, the approximant is a finite sum

$$f_N(x) = \sum_{j=1}^N \alpha_j \sigma(w_j^\top x + b_j), \quad x \in K \subset \mathbb{R}^d, \quad (1)$$

where the parameters are allowed to vary freely. This form is powerful, but it leaves open a practical question: if the data occupy a structured region of space, can the initial weights already encode part of that geometry?

Most standard initializations, including Xavier/Glorot initialization [6], are designed to stabilize signal propagation and gradient scale. They are not intended to represent class geometry before training. For image classification, however, even a simple benchmark such as MNIST has visible class-dependent structure: each digit class has a mean shape, dominant deformation directions, and residual directions that are less stable. The central idea of this work is that initialization need not be blind to such structure.

This paper connects two levels of geometry. The first is a compact constructive background for sigmoidal networks. This work builds on earlier work by Chu and Kuo [2], which developed a planar sigmoidal construction for organizing half-spaces, polytopes, and finite covers through a boundary-first, tropical-geometry-inspired viewpoint. We use this component only as geometric motivation: it explains how prescribed regions can be translated into network weights when the geometry is known explicitly.

The main contribution of this paper is the second level: a data-driven high-dimensional instantiation for image data. Instead of assuming specified planar covers, we estimate class geometry from samples. For each class, we compute a centered SVD/PCA basis [10], select an energy-adaptive rank, and formulate a SVD-based subspace classifier. This classifier is not the neural model; it serves as a geometric reference that tests whether class-wise spectral coordinates already separate the classes.

We then compile the same spectral geometry into a one-hidden-layer sigmoidal MLP. Each retained SVD direction defines a normalized coordinate around a class mean. Compatibility with the class is expressed as a slab constraint on this coordinate, and each slab is represented by two sigmoid gates, one for each side of the interval. Thus the hidden layer is partitioned into class-specific groups, with two hidden units per retained direction, and the output layer initially aggregates the gates belonging to each class. This gives S-GAI, an explicit spectral geometry-aware initializer whose width is controlled by the retained spectral ranks.

Our contributions are:

- We provide a concise bridge from UAT finite sums to smooth half-space and cover-based sigmoid gates, building on the planar sigmoidal construction of [2];
- We introduce a SVD-based subspace classifier that serves as a non-neural reference for testing whether class-wise spectral geometry is discriminative and selecting the proper parameters for S-GAI;
- We propose S-GAI, a data-driven spectral geometry-aware initializer for MLPs, instantiated with class-wise SVD; each retained class direction contributes two hidden units, and the hidden width is determined by an energy threshold τ ;

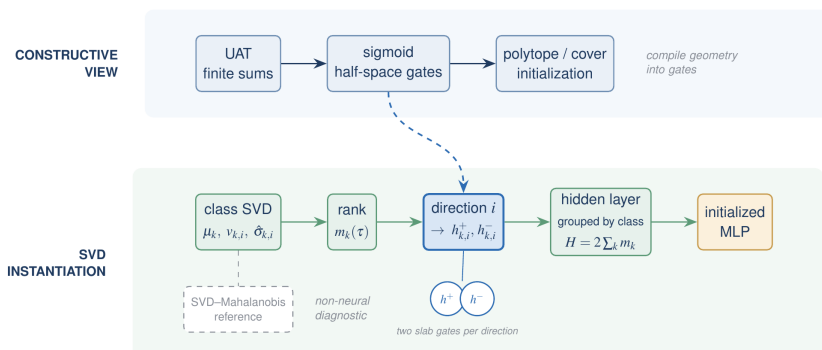


Fig. 1. Method flow. The top row summarizes the constructive view: finite-sum sigmoidal networks can be organized as half-space gates and then as polytope- or cover-based initializers. The bottom row shows the data-driven instantiation used for high-dimensional images. Class-wise SVD estimates the mean, directions, and scales; an energy threshold selects the retained rank $m_k(\tau)$; each retained direction is compiled into two slab gates $h_{k,i}^+$ and $h_{k,i}^-$; and the resulting gates are placed in a class-grouped hidden layer of width $H = 2 \sum_k m_k$. The SVD-based subspace classifier is shown only as a non-neural geometric reference for the selection of energy threshold τ .

- We evaluate S-GAI through matched comparisons with Xavier initialization on MNIST, Fashion-MNIST, and CIFAR-10. Under zero-epoch and frozen-hidden protocols, S-GAI slab gates provide substantially more informative representations than matched random gates, while full training reaches comparable final accuracy under the same architecture and optimizer.

2 From Finite Sums to Geometric Gates

Let $K \subset \mathbb{R}^d$ be compact and let $\sigma(t) = (1 + e^{-t})^{-1}$. Cybenko’s theorem states that finite sums of the form (1) are dense in $C(K)$ for sigmoidal activations [3]; related and extended results were given by Funahashi [5], Hornik *et al.* [9], Hornik [8], Leshno *et al.* [15], and Barron [1]; see also Pinkus [17]. These theorems ensure representability, but they do not specify an initialization tied to a particular decision region.

Following the planar construction in [2], we use the following elementary gate as the geometric primitive. For $a \in \mathbb{R}^d$, $c \in \mathbb{R}$, and sharpness $\kappa > 0$, define

$$g_{a,c,\kappa}(x) = \sigma(\kappa(c - a^\top x)). \quad (2)$$

This unit is close to one inside the half-space $a^\top x \leq c$ and close to zero outside it.

Lemma 1 (Half-space gate). *Let $\delta > 0$. If $c - a^\top x \geq \delta$, then $g_{a,c,\kappa}(x) \geq 1 - \exp(-\kappa\delta)$. If $a^\top x - c \geq \delta$, then $g_{a,c,\kappa}(x) \leq \exp(-\kappa\delta)$.*

Proof. For $t \geq 0$, $\sigma(t) = 1/(1 + e^{-t}) \geq 1 - e^{-t}$. For $t \leq 0$, $\sigma(t) \leq e^t$. Apply these inequalities to $t = \kappa(c - a^\top x)$.

Let a polytope be written as

$$P = \bigcap_{\ell=1}^m \{x : a_\ell^\top x \leq c_\ell\}. \quad (3)$$

Using one gate per supporting half-space, define

$$G_P(x) = \sum_{\ell=1}^m \sigma(\kappa(c_\ell - a_\ell^\top x)) - \left(m - \frac{1}{2}\right). \quad (4)$$

Proposition 1 (Robust polytope classifier). *Assume $m \exp(-\kappa\delta) < 1/2$. If x satisfies all inequalities with margin at least δ , then $G_P(x) > 0$. If x violates at least one inequality with margin at least δ , then $G_P(x) < 0$.*

Proof. Inside P with margin δ , Lemma 1 gives

$$G_P(x) \geq m(1 - e^{-\kappa\delta}) - \left(m - \frac{1}{2}\right) > 0.$$

If one constraint is violated by margin δ , then the corresponding gate is at most $e^{-\kappa\delta}$, while all other gates are at most one. Thus

$$G_P(x) \leq (m - 1) + e^{-\kappa\delta} - \left(m - \frac{1}{2}\right) < 0.$$

Finite unions are obtained by a second sigmoidal aggregation. For $C = \bigcup_{r=1}^R P_r$, define

$$F_C(x) = \sum_{r=1}^R \sigma(\lambda G_{P_r}(x)) - \frac{1}{2}. \quad (5)$$

If x lies robustly inside one component, one term is close to one; if x lies robustly outside all components, all terms are close to zero for sufficiently large λ . This gives a sigmoidal network in the same finite-sum spirit as UAT, but with weights chosen from an explicit geometric description.

The construction is inspired by the way tropical geometry represents polyhedral structure through max-plus affine pieces [16]. ReLU networks inherit closely related piecewise-linear subdivisions and have been studied through tropical rational maps [19]. We do not use ReLU networks; the point is instead to keep a smooth sigmoid activation while borrowing a boundary-first design principle: identify geometric boundary primitives first, then compile them into weights.

For a general compact target region in the plane, one may approximate the region by a finite cover and polygonal components, then apply (4) and (5). The planar examples and visual demonstrations are reported in prior work [2]. In this paper, the role of this section is to motivate the high-dimensional replacement: when the geometry is not hand-specified, estimate it from data.

3 Spectral Class Geometry and SVD-Referenced Subspace Classifier

For image data, class regions are not given as planar covers. We therefore estimate class geometry from the training set. For class k , let $\mu_k \in \mathbb{R}^d$ be the class mean and let $X_k \in \mathbb{R}^{n_k \times d}$ contain centered samples $x_i - \mu_k$. Compute

$$X_k = U_k S_k V_k^\top, \quad V_k = [v_{k,1}, \dots, v_{k,d}], \quad (6)$$

where $S_k = \text{diag}(s_{k,1}, \dots)$. The empirical standard deviation along direction $v_{k,i}$ is

$$\hat{\sigma}_{k,i} = s_{k,i} / \sqrt{n_k - 1}. \quad (7)$$

For an energy threshold $\tau \in (0, 1)$, choose

$$m_k(\tau) = \min \left\{ m : \frac{\sum_{i=1}^m s_{k,i}^2}{\sum_i s_{k,i}^2} \geq \tau \right\}. \quad (8)$$

With $m_k = m_k(\tau)$, the SVD-Mahalanobis reference score is

$$d_k(x) = \sum_{i=1}^{m_k} \left(\frac{v_{k,i}^\top (x - \mu_k)}{\hat{\sigma}_{k,i}} \right)^2 + \lambda \frac{\left\| (I - V_{k,m_k} V_{k,m_k}^\top)(x - \mu_k) \right\|_2^2}{\hat{\sigma}_{k,m_k}^2}, \quad (9)$$

where V_{k,m_k} contains the retained directions and $\lambda \geq 0$ penalizes residual energy outside the retained subspace.

This score defines a subspace classifier based on the estimated SVD geometry of each class. The first term is a truncated Mahalanobis distance inside the retained class subspace: deviations along high-variance class directions are normalized by their empirical spectral scales. The second term measures the normalized residual energy outside the retained subspace. This complement penalty is important because a sample may have moderate coordinates along the retained directions of a class while still being poorly explained by that class subspace as a whole. The residual term therefore acts as a rejection mechanism for samples that lie far from the retained spectral model. Empirically, removing this term by setting $\lambda = 0$ leads to a large accuracy drop of more than 13 percentage points, as shown in Fig. 2.

Classification is by

$$\hat{y}(x) = \arg \min_k d_k(x). \quad (10)$$

The role of this classifier is twofold in this work. First, it provides a non-neural reference for testing whether class-wise spectral geometry is already discriminative. Second, it identifies the retained directions, ranks, and spectral scales that will later be compiled into sigmoid slab gates. In this sense, the classifier is not a competing neural architecture, but a geometric intermediate between the estimated class subspaces and the initialized MLP.

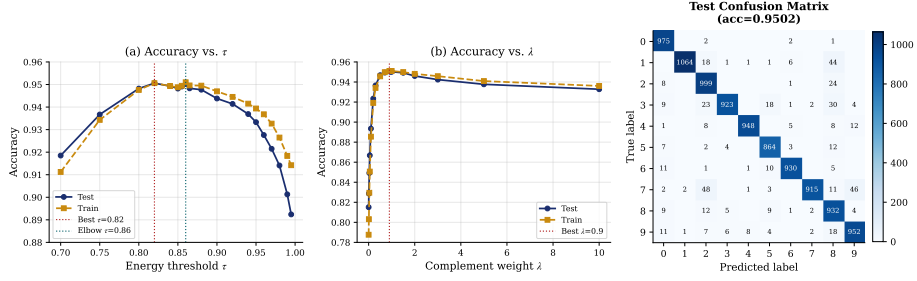


Fig. 2. SVD-based Subspace Classifier reference for MNIST. The energy threshold selects class-dependent ranks, and the complement penalty rejects samples that are not well explained by a class subspace. This reference is non-neural; it is used to validate the spectral geometry before compiling it into an MLP.

4 Compiling Spectral Slabs into a Sigmoid MLP

We now compile the class-wise SVD geometry into a one-hidden-layer sigmoid MLP. We refer to the resulting procedure as S-GAI, short for Spectral Geometry-Aware Initialization. For class k and retained direction i , define the normalized spectral coordinate

$$z_{k,i}(x) = \frac{v_{k,i}^\top(x - \mu_k)}{\hat{\sigma}_{k,i}}. \quad (11)$$

A sample compatible with class k should have moderate values of $z_{k,i}(x)$ along the retained directions. We model the interval $[-\rho, \rho]$ by two sigmoid slab gates:

$$h_{k,i}^+(x) = \sigma(\beta(\rho - z_{k,i}(x))), \quad h_{k,i}^-(x) = \sigma(\beta(\rho + z_{k,i}(x))), \quad (12)$$

where $\rho > 0$ is the slab half-width and $\beta > 0$ controls sharpness. Both gates are near one when $z_{k,i}(x) \in [-\rho, \rho]$.

Equation (12) gives explicit hidden-layer weights:

$$\begin{aligned} w_{k,i}^+ &= -\beta v_{k,i} / \hat{\sigma}_{k,i}, \quad b_{k,i}^+ = \beta\rho + \beta v_{k,i}^\top \mu_k / \hat{\sigma}_{k,i}, \\ w_{k,i}^- &= \beta v_{k,i} / \hat{\sigma}_{k,i}, \quad b_{k,i}^- = \beta\rho - \beta v_{k,i}^\top \mu_k / \hat{\sigma}_{k,i}. \end{aligned} \quad (13)$$

Thus each retained SVD direction contributes two hidden units: one gate for the upper half-space constraint $z_{k,i} \leq \rho$ and one gate for the lower half-space constraint $z_{k,i} \geq -\rho$. The hidden layer is partitioned into class-specific groups,

$$\mathcal{H} = \mathcal{H}_0 | \mathcal{H}_1 | \cdots | \mathcal{H}_9, \quad |\mathcal{H}_k| = 2m_k(\tau),$$

and its total width is

$$H(\tau) = 2 \sum_{k=0}^9 m_k(\tau). \quad (14)$$

The initialized class logit is the normalized average of the class slab responses:

$$\ell_k^{(0)}(x) = \frac{\gamma}{2m_k} \sum_{i=1}^{m_k} (h_{k,i}^+(x) + h_{k,i}^-(x)), \quad (15)$$

with scale $\gamma > 0$.

4.1 Experiment Protocols

After initialization, we study two protocols: *full training*, in which all weights are updated, and *frozen-hidden training*, in which the S-GAI slab gates (the hidden layer) are fixed and only the output layer is trained.

For each dataset and each threshold τ , the Xavier baseline uses exactly the same architecture and hidden width $H(\tau)$. The only difference is the initial value of the weights. In the *full training* protocol, both hidden and output weights are trainable. In the *frozen-hidden training* protocol, the randomly initialized hidden layer is fixed and only the output layer is trained. This isolates the effect of S-GAI’s data-driven spectral geometry from parameter count.

For a one-hidden-layer sigmoid MLP with input dimension d , hidden width H , and 10 outputs, the total parameter count is

$$(dH + H) + (10H + 10) = (d + 11)H + 10. \quad (16)$$

For MNIST and Fashion-MNIST, $d = 784$; for CIFAR-10, $d = 3072$. Under frozen-hidden training, the trainable parameter count is only

$$10H + 10. \quad (17)$$

5 Experiments

5.1 Datasets and Experimental Setup

We evaluate S-GAI on three image-classification datasets. The main controlled study uses MNIST handwritten digits [13, 14], flattened to $x \in \mathbb{R}^{784}$. To test whether the effect is specific to digit shapes, we also evaluate the same protocol on Fashion-MNIST [18], which has the same image size and number of classes as MNIST but contains clothing categories. Finally, we include CIFAR-10 [12] as a more challenging natural-image stress test. For CIFAR-10, we deliberately apply the method directly to flattened raw RGB pixels, $x \in \mathbb{R}^{3072}$, without convolutional inductive bias, data augmentation, or pretrained features.

All neural experiments use one-hidden-layer sigmoidal MLPs trained for 20 epochs with Adam [11]. We repeat all experiments over multiple random seeds and test the energy thresholds $\tau \in \{0.75, 0.86, 0.90, 0.95\}$. For each dataset and each threshold, S-GAI and Xavier models use the same hidden width $H(\tau)$, optimizer, number of epochs, and train/freeze protocol. The highlight threshold is $\tau = 0.95$ for MNIST and Fashion-MNIST. For CIFAR-10, we highlight $\tau = 0.90$, since this setting gives the strongest frozen-hidden representation in our experiments.

Tables 1–4 summarize the experimental evidence. Table 1 reports the retained ranks and induced hidden widths. Table 2 compares the non-neural SVD-Mahalanobis reference with the zero-epoch initialized MLP. Tables 3 and 4 report the matched train/freeze comparisons at the highlight threshold and across thresholds, respectively.

Dataset	τ	Mean rank	Rank range	H	Mean retained energy	Mean cutoff std.
MNIST	0.75	23.9	9–32	478	0.753	0.5643
	0.86	48.4	23–60	968	0.861	0.3348
	0.90	68.2	36–82	1364	0.901	0.2534
	0.95	121.4	71–142	2428	0.950	0.1558
Fashion-MNIST	0.75	18.6	12–41	372	0.754	0.5446
	0.86	50.2	24–96	1004	0.861	0.2890
	0.90	78.2	36–135	1564	0.901	0.2121
	0.95	155.5	73–222	3110	0.950	0.1281
CIFAR-10	0.75	22.3	15–34	446	0.752	1.0229
	0.86	61.6	44–86	1232	0.860	0.5210
	0.90	98.6	74–131	1972	0.900	0.3812
	0.95	206.8	164–267	4136	0.950	0.2196

Table 1. Energy thresholds determine the class-dependent SVD ranks used by both the SVD-based subspace classifier and the S-GAI initializer. The hidden width is $H = 2\sum_k m_k$ because each retained direction gives two sigmoid slab gates. MNIST and Fashion-MNIST are flattened to \mathbb{R}^{784} , while CIFAR-10 is flattened to \mathbb{R}^{3072} .

Dataset	τ	H	SVD-Mahalanobis(%)	S-GAI init(%)
MNIST	0.75	478	93.67	45.53
	0.86	968	95.02	81.35
	0.90	1364	94.38	86.17
	0.95	2428	93.33	87.41
Fashion-MNIST	0.75	372	67.42	56.34
	0.86	1004	74.43	62.54
	0.90	1564	78.41	66.91
	0.95	3110	83.03	71.32
CIFAR-10	0.75	446	23.20	20.49
	0.86	1232	24.14	20.39
	0.90	1972	27.19	20.32
	0.95	4136	32.46	18.51

Table 2. Geometry-only performance before gradient updates. The SVD-Mahalanobis column reports the non-neural SVD-based subspace reference classifier using Eq. (9). S-GAI init reports the zero-epoch test accuracy of the S-GAI-initialized MLP.

5.2 Results

The key comparison is not S-GAI against a smaller or larger network; it is S-GAI against a matched Xavier network with the same architecture. Across datasets, S-GAI starts from a substantially more informative state than Xavier initialization. At $\tau = 0.95$, the zero-epoch S-GAI-initialized model reaches 87.41% test accuracy on MNIST and 71.32% on Fashion-MNIST, while the matched Xavier models remain near chance level. On CIFAR-10, where we highlight $\tau = 0.90$ for the raw-pixel stress test, the S-GAI-initialized model reaches 20.32% before training, compared with 9.97% for Xavier.

Under full training, S-GAI-initialized and Xavier-initialized models reach similar final accuracy. This suggests that S-GAI is not simply increasing capacity; rather, it changes the starting representation while keeping the architecture fixed. The frozen-hidden setting is more diagnostic: when the hidden layer cannot be trained, strong performance indicates that the initialized S-GAI slab gates already form useful features. At $\tau = 0.95$, frozen S-GAI slab gates reach

Dataset	Model	H	Trainable params	Init acc.(%)	Final acc.(%)
MNIST	S-GAI (full)	2428	1,930,270	87.41	98.02 \pm 0.05
	Xavier (full)	2428	1,930,270	10.42 \pm 0.78	97.90 \pm 0.08
	S-GAI (frozen)	2428	24,290	87.41	96.73 \pm 0.13
	Xavier (frozen)	2428	24,290	10.42 \pm 0.78	89.31 \pm 0.56
Fashion-MNIST	S-GAI (full)	3110	2,472,460	71.32	89.00 \pm 0.24
	Xavier (full)	3110	2,472,460	10.01 \pm 0.01	88.37 \pm 0.22
	S-GAI (frozen)	3110	31,110	71.32	86.36 \pm 0.56
	Xavier (frozen)	3110	31,110	10.01 \pm 0.01	80.52 \pm 0.31
CIFAR-10	S-GAI (full)	1972	6,079,686	20.32	52.11 \pm 0.82
	Xavier (full)	1972	6,079,686	9.97 \pm 0.04	52.16 \pm 0.08
	S-GAI (frozen)	1972	19,730	20.32	44.36 \pm 0.59
	Xavier (frozen)	1972	19,730	9.97 \pm 0.04	36.53 \pm 0.08

Table 3. Matched MLP comparison at the highlight threshold $\tau = 0.95$ for MNIST and Fashion-MNIST, and $\tau = 0.90$ for CIFAR-10. Within each dataset, S-GAI and Xavier models use the same architecture and hidden width; they differ only in initialization and whether the hidden layer is trainable. The frozen rows test the quality of the initialized representation itself.

Dataset	τ	H	S-GAI full(%)	Xavier full(%)	S-GAI frozen(%)	Xavier frozen(%)
MNIST	0.75	478	97.45 \pm 0.03	97.91 \pm 0.04	91.48 \pm 0.15	88.44 \pm 0.13
	0.86	968	97.73 \pm 0.03	98.00 \pm 0.08	95.11 \pm 0.22	89.34 \pm 0.20
	0.90	1364	97.84 \pm 0.11	97.95 \pm 0.09	96.05 \pm 0.24	89.46 \pm 0.30
	0.95	2428	98.02 \pm 0.05	97.90 \pm 0.08	96.73 \pm 0.13	89.31 \pm 0.56
Fashion-MNIST	0.75	372	87.89 \pm 0.22	88.21 \pm 0.11	78.91 \pm 0.28	78.65 \pm 0.12
	0.86	1004	88.73 \pm 0.15	88.55 \pm 0.12	83.94 \pm 0.27	79.88 \pm 0.39
	0.90	1564	88.81 \pm 0.50	88.03 \pm 0.40	85.14 \pm 0.87	79.93 \pm 0.41
	0.95	3110	89.00 \pm 0.24	88.37 \pm 0.22	86.36 \pm 0.56	80.52 \pm 0.31
CIFAR-10	0.75	446	51.17 \pm 0.46	50.31 \pm 0.33	39.93 \pm 0.04	35.18 \pm 0.31
	0.86	1232	52.83 \pm 0.39	51.50 \pm 0.65	40.94 \pm 1.56	37.22 \pm 0.56
	0.90	1972	52.11 \pm 0.82	52.16 \pm 0.08	44.36 \pm 0.59	36.53 \pm 0.08
	0.95	4136	52.98 \pm 1.45	51.65 \pm 0.25	38.84 \pm 2.94	36.47 \pm 0.69

Table 4. Effect of the energy threshold on matched-protocol accuracy across datasets. Fully trainable models reach similar final accuracy, while the frozen-hidden comparison consistently favors S-GAI slab gates over frozen random gates. CIFAR-10 is evaluated directly on flattened raw pixels and therefore serves as a natural-image stress test.

96.73% on MNIST and 86.36% on Fashion-MNIST, compared with 89.31% and 80.52% for frozen random gates. On CIFAR-10, the strongest frozen-hidden advantage appears at $\tau = 0.90$, where S-GAI (frozen) reaches 44.36%, compared with 36.53% for frozen random gates. This is consistent with the interpretation in [2] that geometry-informed initialization can shift part of training from discovering decision boundaries from scratch toward calibrating and refining an already structured representation.

Figs. 3–5 summarize the same behavior from complementary views. The parameter-count and energy-rank plots show that fully trainable models are comparable after optimization, while the frozen-hidden comparison consistently favors S-GAI. Fig. 6 provides a direct diagnostic view through confusion matrices and error galleries. The remaining errors are mostly plausible class confusions, and the before-training confusion matrices show that S-GAI already induces structured predictions before gradient updates on MNIST and Fashion-MNIST.

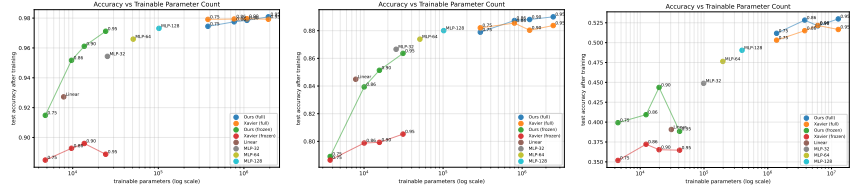


Fig. 3. Accuracy versus trainable parameter count on MNIST, Fashion-MNIST, and CIFAR-10, shown from left to right. S-GAI and Xavier use matched hidden width at each energy threshold. Fully trainable models reach similar final accuracy, while the frozen-hidden comparison evaluates the quality of the fixed hidden representation.

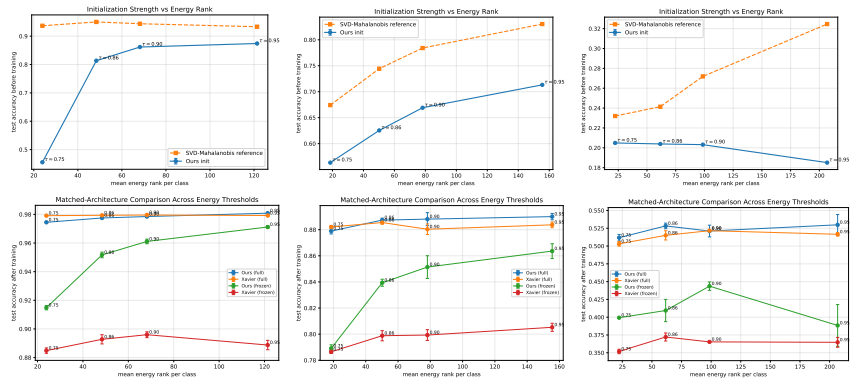


Fig. 4. Energy-rank analysis on MNIST, Fashion-MNIST, and CIFAR-10, shown from left to right. Top: before training, S-GAI is already more informative than random initialization. Bottom: after training, fully trainable models are close, while the frozen-hidden setting reveals the representation value of the S-GAI slab gates.

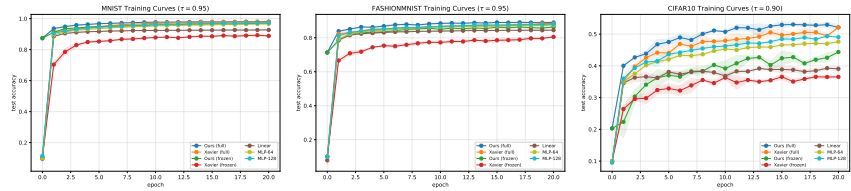


Fig. 5. Training curves on MNIST, Fashion-MNIST, and CIFAR-10, shown from left to right. MNIST and Fashion-MNIST use $\tau = 0.95$, while CIFAR-10 uses $\tau = 0.90$ as a raw-pixel stress test. Across datasets, S-GAI starts from a more informative state than the matched Xavier initialization. Under full training, the models reach similar final accuracy, while the frozen-hidden protocol highlights the representation quality of S-GAI.

On the more challenging CIFAR-10 benchmark, this structure is weaker, but the initialized model remains above chance and avoids the degenerate single-class prediction pattern observed under Xavier initialization. After full training, both initializations reach comparable accuracy as in the other cases.

6 Discussion and Limitations

The proposed construction connects two levels of geometry. At the UAT level, half-space gates and finite covers show how a sigmoidal MLP can be programmed from a target region. At the practical image level, class-wise SVD estimates dominant directions and spectral scales directly from samples. The energy threshold τ becomes a practical complexity knob: small τ gives a coarse class model and fewer gates, while large τ retains finer variation and uses more parameters.

The cross-dataset results support this interpretation. On MNIST and Fashion-MNIST, S-GAI-initialized networks are already strongly discriminative before training, and the frozen-hidden protocol shows a clear advantage over frozen random gates. On CIFAR-10, the effect is weaker but still informative under the flattened raw-pixel setting.

The non-neural SVD-Mahalanobis subspace classifier also provides a useful diagnostic for the applicability of S-GAI. It uses the same class-wise means, spectral directions, spectral scales, and retained ranks before they are compiled into sigmoid slab gates. Therefore, its performance indicates whether the estimated input-space spectral geometry is already discriminative. This helps explain the cross-dataset trend: the method is strongest on MNIST and Fashion-MNIST, where the spectral reference is already informative, and weaker on CIFAR-10, where class identity depends more on local texture, pose, background, and higher-level visual features. The CIFAR-10 result therefore delineates the current regime of the method rather than simply serving as a failure case.

There are also clear limitations. The SVD geometry is class-wise and linear; it does not model nonlinear manifolds inside each class. The slab construction treats retained directions independently and therefore approximates an axis-aligned spectral polytope in each class basis rather than the full data distribution. Finally, all experiments use low-resolution benchmarks and one-hidden-layer sigmoidal MLPs. A natural next step is to transfer the initialization principle to learned feature spaces and architectures with stronger visual inductive bias, such as convolutional neural networks [7, 13] and Vision Transformers [4].

7 Conclusion

We presented a geometry-aware initialization framework for sigmoidal MLPs. Starting from the original finite-sum form of UAT, we summarized how smooth half-space and cover gates can be constructed from target geometry. For high-dimensional image data, we estimated class geometry with SVD, formulated a SVD-Mahalanobis subspace classifier as a non-neural geometric reference, and compiled retained spectral directions into pairs of sigmoid slab gates. This gives

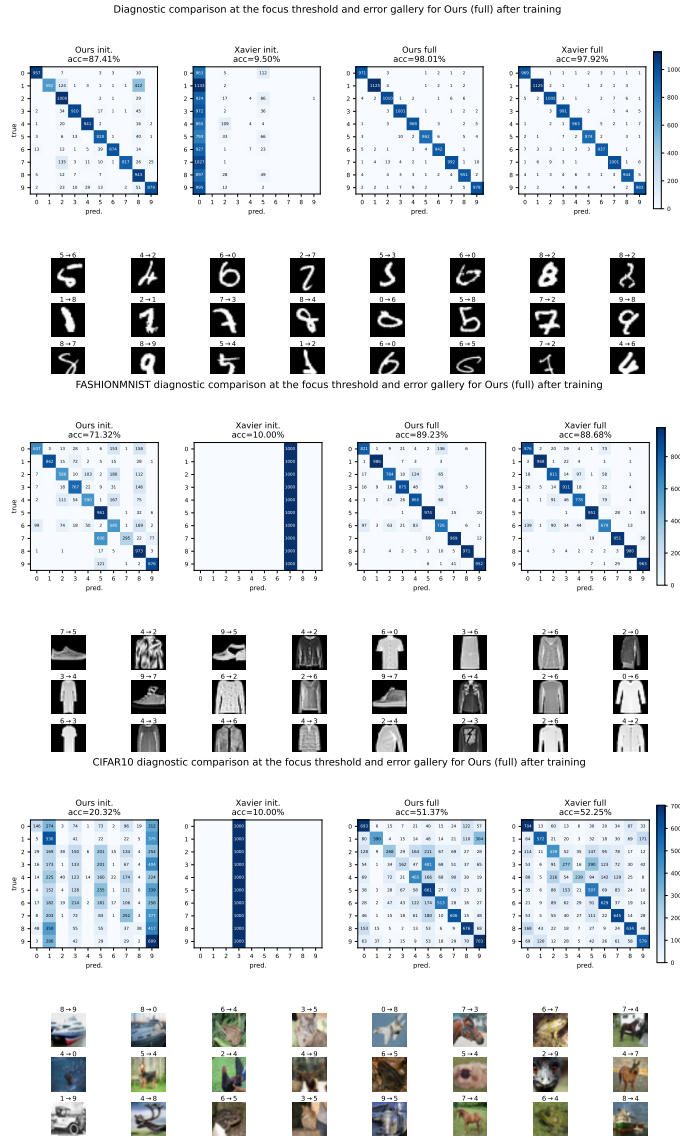


Fig. 6. Diagnostic comparison on MNIST, Fashion-MNIST, and CIFAR-10, shown from top to bottom. The MNIST and Fashion-MNIST results use $\tau = 0.95$, while CIFAR-10 uses $\tau = 0.90$, where the frozen-hidden representation is strongest. For each dataset, the four confusion matrices compare S-GAI and the matched Xavier baseline before training and after full training. The error gallery shows representative misclassified test images from S-GAI after full training. Across datasets, fully trained S-GAI-initialized and Xavier-initialized models reach similar final accuracy, while the initialized S-GAI slab gates already induce structured predictions before optimization, especially on MNIST and Fashion-MNIST.

an explicit data-geometry-to-weights procedure for initializing the hidden layer of a one-hidden-layer sigmoid network.

The experiments compare S-GAI against matched Xavier baselines across MNIST, Fashion-MNIST, and CIFAR-10. Under full training, S-GAI-initialized and Xavier-initialized models reach comparable final accuracy, so the main contribution is not a larger-capacity classifier. The clearest evidence appears before and under constrained training: S-GAI starts from a much more informative state, and when the hidden layer is frozen, class-wise spectral gates are consistently more useful than the matched frozen Xavier baseline. These results support the view that empirical class geometry can be injected into a sigmoidal MLP before gradient-based training, while the CIFAR-10 stress test suggests that future work should extend the same principle to feature-space and convolutional settings.

References

1. Barron, A.R.: Universal approximation bounds for superpositions of a sigmoidal function. *IEEE Transactions on Information Theory* **39**(3), 930–945 (1993). <https://doi.org/10.1109/18.256500> 3
2. Chu, Y.S., Kuo, Y.C.: From universal approximation theorem to tropical geometry of multi-layer perceptrons (2025). <https://doi.org/10.48550/arXiv.2510.15012>, <https://arxiv.org/abs/2510.15012> 2, 3, 4, 9
3. Cybenko, G.: Approximation by superpositions of a sigmoidal function. *Mathematics of Control, Signals and Systems* **2**(4), 303–314 (1989). <https://doi.org/10.1007/BF02551274> 1, 3
4. Dosovitskiy, A., Beyer, L., Kolesnikov, A., Weissenborn, D., Zhai, X., Unterthiner, T., Dehghani, M., Minderer, M., Heigold, G., Gelly, S., Uszkoreit, J., Houlsby, N.: An image is worth 16x16 words: Transformers for image recognition at scale. In: *International Conference on Learning Representations* (2021) 11
5. Funahashi, K.I.: On the approximate realization of continuous mappings by neural networks. *Neural Networks* **2**(3), 183–192 (1989). [https://doi.org/10.1016/0893-6080\(89\)90003-8](https://doi.org/10.1016/0893-6080(89)90003-8) 3
6. Glorot, X., Bengio, Y.: Understanding the difficulty of training deep feedforward neural networks. In: *Proceedings of the Thirteenth International Conference on Artificial Intelligence and Statistics. JMLR Workshop and Conference Proceedings*, vol. 9, pp. 249–256 (2010), <https://proceedings.mlr.press/v9/glorot10a.html> 2
7. He, K., Zhang, X., Ren, S., Sun, J.: Deep residual learning for image recognition. In: *Proceedings of the IEEE Conference on Computer Vision and Pattern Recognition*. pp. 770–778 (2016) 11
8. Hornik, K.: Approximation capabilities of multilayer feedforward networks. *Neural Networks* **4**(2), 251–257 (1991). [https://doi.org/10.1016/0893-6080\(91\)90009-T](https://doi.org/10.1016/0893-6080(91)90009-T) 3
9. Hornik, K., Stinchcombe, M., White, H.: Multilayer feedforward networks are universal approximators. *Neural Networks* **2**(5), 359–366 (1989). [https://doi.org/10.1016/0893-6080\(89\)90020-8](https://doi.org/10.1016/0893-6080(89)90020-8) 3
10. Jolliffe, I.T.: *Principal Component Analysis*. Springer, 2 edn. (2002). <https://doi.org/10.1007/b98835> 2

11. Kingma, D.P., Ba, J.: Adam: A method for stochastic optimization. In: International Conference on Learning Representations (2015), <https://arxiv.org/abs/1412.6980> 7
12. Krizhevsky, A.: Learning multiple layers of features from tiny images. Tech. rep., University of Toronto (2009), <https://www.cs.toronto.edu/~kriz/learning-features-2009-TR.pdf> 7
13. LeCun, Y., Bottou, L., Bengio, Y., Haffner, P.: Gradient-based learning applied to document recognition. *Proceedings of the IEEE* **86**(11), 2278–2324 (1998). <https://doi.org/10.1109/5.726791> 7, 11
14. LeCun, Y., Cortes, C., Burges, C.J.C.: MNIST handwritten digit database. <http://yann.lecun.com/exdb/mnist/> (2010) 7
15. Leshno, M., Lin, V.Y., Pinkus, A., Schocken, S.: Multilayer feedforward networks with a nonpolynomial activation function can approximate any function. *Neural Networks* **6**(6), 861–867 (1993). [https://doi.org/10.1016/S0893-6080\(05\)80131-5](https://doi.org/10.1016/S0893-6080(05)80131-5) 3
16. Maclagan, D., Sturmfels, B.: Introduction to Tropical Geometry, Graduate Studies in Mathematics, vol. 161. American Mathematical Society (2015) 4
17. Pinkus, A.: Approximation theory of the MLP model in neural networks. *Acta Numerica* **8**, 143–195 (1999). <https://doi.org/10.1017/S0962492900002919> 3
18. Xiao, H., Rasul, K., Vollgraf, R.: Fashion-mnist: a novel image dataset for benchmarking machine learning algorithms. arXiv preprint arXiv:1708.07747 (2017) 7
19. Zhang, L., Naitzat, G., Lim, L.H.: Tropical geometry of deep neural networks. In: Proceedings of the 35th International Conference on Machine Learning. Proceedings of Machine Learning Research, vol. 80, pp. 5824–5832 (2018), <https://proceedings.mlr.press/v80/zhang18i.html> 4